ANCF Multiplicative-Decomposition Thermoelastic Approach for Arbitrary Geometry

Ahmed A. Shabana[1] and Dayu Zhang[2]

Abstract: The classical approach for the thermal analysis of solids and fluids uses the strain additive decomposition to account for the effect of the temperature. This strain-based approach does not properly capture the effect of complex stress-free reference-configuration geometry, is applicable only to small deformation problems, and leads to simplified expression for the Green–Lagrange strain tensor. In view of the geometric description of the absolute nodal coordinate formulation (ANCF), a new ANCF gradient-based approach is proposed. This approach employs a multiplicative decomposition of the matrix of position-gradient vectors in the stress-free reference configuration into two position-gradient matrices. One matrix is associated with the reference-configuration geometry before the application of the thermal load, and the other accounts for the volumetric change due to the change in temperature. A numerical study demonstrated the implementation of the proposed gradient-based approach. **DOI: 10.1061/(ASCE)ST.1943-541X.0003001.**

Author keywords: Thermal analysis; Reference-configuration geometry; Position gradients; Absolute nodal coordinate formulation (ANCF); Poisson effect.

Introduction

The analysis of the effect of thermal loads has been the subject of many investigations in solid and fluid mechanics applications (Chang et al. 1999; Cui et al. 2019; API 2004; Errara and Chemin 2013; Perelman 1961; Dorfman and Renner 2009; Roe et al. 2008, 2007; Henshaw and Chand 2009; Helselhaus et al. 1992; Ojas and Leyland 2014). If the change in the material properties due to the change in temperature is not considered, thermal expansion is a stress-free process that has no effect on the formulation of the elastic forces of a continuum. The elastic strains used in the constitutive relationships are not function of the volumetric change produced by the thermal load. The classical approach for the thermal analysis of solids and fluids uses the strain additive decomposition to account for the effect of the environment temperature (Cook 1981). This strain-based approach does not properly capture the effect of complex stress-free reference-configuration geometry, is applicable only to small deformation problems, and leads to simplified strain expressions. Furthermore, conventional finite-element (FE) formulations employ low-order interpolations or rotation-based elements that cannot be used to describe accurately complex geometric shapes. The displacement fields of these elements are not related by a linear mapping to computational geometry methods such as B-splines and non uniform rational B-spline (NURBS) (Piegl and Tiller 1997; Farin 1999; Rogers 2001; Gallier 2011; Goetz 1970; Kreyszig 1991). Because of these limitations, there is no approach in the literature that can be used to properly integrate thermal analysis and complex stress-free reference-configuration geometries. Such an integration cannot be achieved using a linear theory based on the principle of superposition or the additive strain decomposition.

The displacement field of the absolute nodal coordinate formulation (ANCF), on the other hand, allows for accurate description of the reference-configuration geometry. This is attributed to the fact that position gradients are used as nodal coordinates (Chen et al. 2019; Tian et al. 2009; Dmitrochenko and Pogorelov 2003; Mikkola and Shabana 2003; Shen et al. 2013; Pan and Cao 2020; Orzechowski 2012; Orzechowski and Frączek 2012; Khan and Anderson 2013; Kłodowski et al. 2011; Nachbagauer et al. 2011; Nachbagauer 2013; Olshevskiy et al. 2014; Nachbagauer 2014; Laflin et al. 2014; Orzechowski and Frączek 2015; Yoo et al. 2004; Takahashi et al. 2005; Lee and Park 2012; Shabana 2018; Fotland et al. 2019; Li et al. 2019; Yu et al. 2010; Yamano et al. 2020; Hewlett 2019; Hewlett et al. 2020; Shen et al. 2020; Htun et al. 2020; Obrezkov et al. 2021). By changing the length and orientation of the nodal position-gradient vectors, which can be used conveniently for local shape manipulations, complex geometries can be described accurately. Furthermore, the ANCF displacement fields are related by a linear mapping to B-splines and NURBS. Therefore, these elements can be used to develop a new procedure for the thermal analysis that accounts for the reference-configuration geometry.

This paper proposes a new computational ANCF gradient-based approach that employs a multiplicative decomposition of the matrix of position-gradient vectors for the solution of the thermos-elasticity problem (Lubarda 2004; Vujosevic and Lubarda 2002; Darijani and Naghdabadi 2013). The proposed multiplicative decomposition uses two gradient matrices; one matrix is associated with the reference-configuration geometry before the application of the thermal load, and the other matrix accounts for the volumetric change due to the temperature variation. Four configurations are used to develop the kinematics of the approach used in this paper; the straight configuration, the stress-free reference configuration, the stress-free thermally expanded configuration, and the current configuration. The approach proposed in this study can account for geometric nonlinearities, is not based on additive decomposition or the principle of superposition, does not use any form of linearization, and can account for arbitrary variation of the temperature.

[1]Professor, Dept. of Mechanical and Industrial Engineering, Univ. of Illinois at Chicago, 842 West Taylor St., Chicago, IL 60607 (corresponding author). Email: shabana@uic.edu

[2]Postdoctor, School of Astronautics, Northwestern Polytechnical Univ., Xi'an, Shaanxi 710072, PR China. Email: dyzhang@mail.nwpu.edu.cn

Note. This manuscript was submitted on July 5, 2020; approved on January 7, 2021; published online on April 23, 2021. Discussion period open until September 23, 2021; separate discussions must be submitted for individual papers. This paper is part of the ***Journal of Structural Engineering***, © ASCE, ISSN 0733-9445.

Numerical results demonstrate the implementation of the gradient-based approach in the thermal analysis and shed light on some of the limitations of existing beam formulations.

Thermal Expansion and Geometry Description

The geometry and kinematics of a continuum in the thermal analysis can be described using four different configurations (Fig. 1): the straight configuration, reference configuration, thermally expanded configuration, and current configurations. Both reference and thermally expanded configurations are assumed to be stress-free. The reference configuration is the continuum configuration before the application of the thermal load, whereas the thermally expanded configuration is the configuration after the application of the thermal load. If the temperature varies, the thermally expanded configuration can change with time.

These four configurations are defined by the coordinates $\mathbf{x} = [x_1 \quad x_2 \quad x_3]^T$, $\mathbf{X} = [X_1 \quad X_2 \quad X_3]^T$, $\mathbf{X}_\Theta = [X_{\Theta 1} \quad X_{\Theta 2} \quad X_{\Theta 3}]^T$, and $\mathbf{r} = [r_1 \quad r_2 \quad r_3]^T$ (Fig. 1). The volumes in the straight, reference, thermally expanded, and current configurations are denoted, respectively, V, V_o, V_Θ, and v. A line element $d\mathbf{r}$ in the current configuration can be written

$$d\mathbf{r} = \frac{\partial \mathbf{r}}{\partial \mathbf{X}} d\mathbf{X} = \mathbf{J} d\mathbf{X} = \left[\left(\frac{\partial \mathbf{r}}{\partial \mathbf{X}_\Theta}\right)\left(\frac{\partial \mathbf{X}_\Theta}{\partial \mathbf{X}}\right)\right]\left(\frac{\partial \mathbf{X}}{\partial \mathbf{x}}\right) d\mathbf{x} = \mathbf{J}_{r\Theta}\mathbf{J}_{\Theta X}\mathbf{J}_o d\mathbf{x} \tag{1}$$

Alternatively, one can write

$$d\mathbf{r} = \frac{\partial \mathbf{r}}{\partial \mathbf{X}_\Theta} d\mathbf{X}_\Theta = \mathbf{J}_{r\Theta} d\mathbf{X}_\Theta = \mathbf{J}\left(\frac{\partial \mathbf{X}_\Theta}{\partial \mathbf{x}}\right) d\mathbf{x} = \mathbf{J}\mathbf{J}_{o+\Theta} d\mathbf{x} \tag{2}$$

where $\mathbf{J}_{r\Theta} = \partial \mathbf{r}/\partial \mathbf{X}_\Theta$, $\mathbf{J}_{\Theta X} = \partial \mathbf{X}_\Theta/\partial \mathbf{X}$, $\mathbf{J}_{o+\Theta} = \partial \mathbf{X}_\Theta/\partial \mathbf{x}$, and $\mathbf{J}_o = \mathbf{J}_{Xx} = \partial \mathbf{X}/\partial \mathbf{x}$. In this case, the matrix of position vector gradients $\mathbf{J}$ that enters into the definition of the elastic Green–Lagrange strain tensor is defined as

$$\mathbf{J} = \partial \mathbf{r}/\partial \mathbf{X}_\Theta = \mathbf{J}_{r\Theta} \tag{3}$$

Using this description, one can have two different representations of the vector $\mathbf{r}$; one is based on the reference configuration $\mathbf{X}$ as $\mathbf{r}(\mathbf{X}, t) = \mathbf{X} + \mathbf{u}(\mathbf{X}, t)$, where $\mathbf{u}$ is the displacement vector, and the other is based on the thermally expanded configuration $\mathbf{X}_\Theta$ as $\mathbf{r}(\mathbf{X}_\Theta, t) = \mathbf{X}_\Theta(\mathbf{X}, t) + \mathbf{u}(\mathbf{X}_\Theta, t)$, this is with the understanding that the displacement vector in this equation differs from the displacement vector used when the reference configuration is used. In the case of zero thermal load, the two configurations are identical, that is, $\mathbf{X}_\Theta = \mathbf{X}$ and $\mathbf{J}_{r\Theta} = \partial \mathbf{r}/\partial \mathbf{X}$, $\mathbf{J}_{\Theta X} = \partial \mathbf{X}_\Theta/\partial \mathbf{X} = \mathbf{I}$, where $\mathbf{I}$ is a 3×3 identity matrix. Contrary to the description used in continuum mechanics in the definition of the position vector $\mathbf{r}$, the configuration defined by $\mathbf{X}_\Theta$ is not fixed, that is $\mathbf{X}_\Theta = \mathbf{X}_\Theta(\mathbf{X}, t)$.

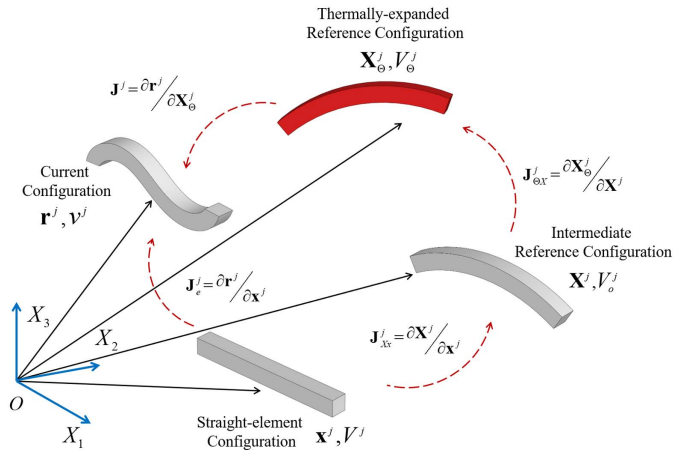

Fig. 1. Thermal expansion configurations.

In the case of constant environment temperature, one can consider $\mathbf{X}_\Theta$ as the reference configuration and write

$$d\mathbf{r} = \frac{\partial \mathbf{r}}{\partial \mathbf{X}_\Theta} d\mathbf{X}_\Theta = \mathbf{J} d\mathbf{X} = \left(\frac{\partial \mathbf{r}}{\partial \mathbf{X}_\Theta}\right)\left[\left(\frac{\partial \mathbf{X}_\Theta}{\partial \mathbf{X}}\right)\left(\frac{\partial \mathbf{X}}{\partial \mathbf{x}}\right)\right] d\mathbf{x} = \mathbf{J}\mathbf{J}_{\Theta X}\mathbf{J}_o d\mathbf{x} = \mathbf{J}\mathbf{J}_{o+\Theta} d\mathbf{x} \tag{4}$$

where in this case matrix $\mathbf{J}$ is redefined, for simplicity, as

$$\mathbf{J} = \partial \mathbf{r}/\partial \mathbf{X}_\Theta, \qquad \mathbf{J}_{o+\Theta} = \mathbf{J}_{\Theta X}\mathbf{J}_o \tag{5}$$

The use of these definitions allows considering the effect of constant temperatures from the outset at a preprocessing stage to reduce the mathematical operations during the process of solving the governing equations. In this case, one can write $dv = |\mathbf{J}\mathbf{J}_{o+\Theta}| dV = |\mathbf{J}||\mathbf{J}_{o+\Theta}| dV$.

If the thermal load is applied before the reference configuration geometry is created, as in the case of heat treatment and manufacturing processes, one can write

$$d\mathbf{r} = \frac{\partial \mathbf{r}}{\partial \mathbf{X}} d\mathbf{X} = \mathbf{J} d\mathbf{X} = \left(\frac{\partial \mathbf{r}}{\partial \mathbf{X}}\right)\left(\frac{\partial \mathbf{X}}{\partial \mathbf{X}_\Theta}\right)\left(\frac{\partial \mathbf{X}_\Theta}{\partial \mathbf{x}}\right) d\mathbf{x} = \mathbf{J}\mathbf{J}_{X\Theta}\mathbf{J}_{\Theta x} d\mathbf{x} \tag{6}$$

where $\mathbf{J}_{X\Theta} = \partial \mathbf{X}/\partial \mathbf{X}_\Theta$, and $\mathbf{J}_{\Theta x} = \partial \mathbf{X}_\Theta/\partial \mathbf{x}$. One also can write

$$d\mathbf{r} = \frac{\partial \mathbf{r}}{\partial \mathbf{X}} d\mathbf{X} = \mathbf{J}_e \mathbf{J}_o^{-1} d\mathbf{x} \tag{7}$$

where

$$\mathbf{J}_o = \frac{\partial \mathbf{X}}{\partial \mathbf{x}} = \frac{\partial \mathbf{X}}{\partial \mathbf{X}_\Theta}\frac{\partial \mathbf{X}_\Theta}{\partial \mathbf{x}} = \mathbf{J}_{X\Theta}\mathbf{J}_{\Theta x} \tag{8}$$

The unique geometric meaning of the position gradients as tangent to coordinate lines was used in this study to develop a general procedure for accounting for the temperature effect (Spencer 1980; Ogden 1984; Bonet and Wood 1997; Bower 2009; Shabana 2018). Displacement gradients do not have the same geometric meaning (Shabana 2015).

In many engineering applications, the reference configuration can have complex geometry that makes it difficult performing the integration and differentiation. Use of the finite-element straight configuration facilitates performing the integration and differentiation without the need for using curved coordinates. This can be achieved, as described in this paper, by using the determinant of the matrix of position gradients $\mathbf{J}_o$ which defines the reference configuration geometry and allows using the x and y coordinates used in the formulation of the finite-element displacement field. This procedure has been adopted in the classical FE literature with isoparametric finite elements.

Conventional Strain-Based Thermal Expansion Approach

In the classical FE literature, the strain additive decomposition often is used in the small deformation analysis and to account for the

temperature effect (Zienkewiez 1977; Zienkiewicz and Taylor 2000). The strain additive decomposition, which is based on the principle of super-position, can be used only with the small strain assumptions. In this case, displacement gradients (not position gradients) are used to represent the strains and directly account for the thermal expansion, as is explained in this study. The strain additive decomposition does not take into consideration the effect of the reference-configuration geometry, which can be complex in solid and fluid applications. When the small strain assumptions are used, the normal strains are approximated as the displacement gradients as $\varepsilon_{ii} = \partial u_i/\partial x_i\,(i = 1, 2, 3)$, where $\mathbf{u} = [u_1 \;\; u_2 \;\; u_3]^T$ is the displacement vector. In this case, the strains are approximated as displacement gradients, and the use of such a linearization does not allow generalization of the approach to large displacement problems. Furthermore, this approach does not accurately capture the reference-configuration geometry using the assumed FE displacement field, particularly when using conventional elements that employ rotations as nodal coordinates.

Strain Additive Decomposition

The classical FE literature assumes that the constant environment temperature can directly influence the Green–Lagrange normal strain components, which are defined using the tensor $\boldsymbol{\varepsilon} = (\mathbf{J}^T\mathbf{J} - \mathbf{I})/2$. The total strain is assumed to be equal to the sum of the elastic strain $\boldsymbol{\varepsilon}_e$ and the stress-free thermal strain $\boldsymbol{\varepsilon}_\Theta$, that is, $\boldsymbol{\varepsilon} = \boldsymbol{\varepsilon}_e + \boldsymbol{\varepsilon}_\Theta$. The total strain, which can be written in a Voigt vector form using the normal strains (ε_{ii}, $i = 1, 2, 3$) and shear strains (ε_{ij}, $i \neq j$, $i, j = 1, 2, 3$) as $(\boldsymbol{\varepsilon})_v = [\varepsilon_{11} \;\; \varepsilon_{22} \;\; \varepsilon_{33} \;\; \varepsilon_{12} \;\; \varepsilon_{13} \;\; \varepsilon_{23}]^T$, is assumed to be known from the solution of the system equations of motion. The strains due to the thermal expansion leads to volumetric change and, in the strain-based approach, such thermal strains are written in terms of the coefficients of thermal expansion and change in temperature. The stress-free thermal strain can be written in vector form as $(\boldsymbol{\varepsilon}_\Theta)_v = [\alpha_{\Theta 1}\Delta\Theta \;\; \alpha_{\Theta 2}\Delta\Theta \;\; \alpha_{\Theta 3}\Delta\Theta \;\; 0 \;\; 0 \;\; 0]^T$, where $\alpha_{\Theta i}(i = 1, 2, 3)$ are the coefficients of thermal expansion, and $\Delta\Theta$ is the constant temperature change (Cook 1981). Therefore, the elastic strain vector can be written as

$$(\boldsymbol{\varepsilon}_e)_v = (\boldsymbol{\varepsilon})_v - (\boldsymbol{\varepsilon}_\Theta)_v = [\,(\varepsilon_{11} - \alpha_{\Theta 1}\Delta\Theta) \quad (\varepsilon_{22} - \alpha_{\Theta 2}\Delta\Theta) \quad (\varepsilon_{33} - \alpha_{\Theta 3}\Delta\Theta) \quad \varepsilon_{12} \quad \varepsilon_{13} \quad \varepsilon_{23}\,]^T \tag{9}$$

It is clear that this approach is based on the strain additive decomposition, which is not suited for complex geometry and nonlinear problems.

Thermal Expansion and Gradients

Assuming that the element straight configuration is the reference-configuration ($\mathbf{X} = \mathbf{x}$), the matrix of position-gradient vectors $\mathbf{J}$ can be written in terms of the matrix of displacement-gradient vectors $\mathbf{J}_d = \partial\mathbf{u}/\partial\mathbf{x}$ as $\mathbf{J} = \mathbf{J}_d + \mathbf{I}$. Because position gradients are not used as element nodal coordinates in the conventional FE approach, the element displacement field cannot be used to describe complex reference-configuration geometries. Therefore, at the initial configuration before displacements, the normal elastic strains are $(\varepsilon_e)_{kk} = (\partial u_k/\partial x_k) - \alpha_{\Theta k}\Delta\Theta = 0$, where $k = 1, 2, 3$, and one can write $(\mathbf{J}_d)_o = \boldsymbol{\alpha}_\Theta\Delta\Theta$, where $\boldsymbol{\alpha}_\Theta$ is a diagonal matrix whose diagonal elements are the coefficients of thermal expansion $\alpha_{\Theta k}$, where $k = 1, 2, 3$. Using this interpretation and the equation $\mathbf{J} = \mathbf{J}_d + \mathbf{I}$, the matrix of position-gradient vectors can be written $(\mathbf{J})_o = (\mathbf{J}_d)_o + \mathbf{I} = \boldsymbol{\alpha}_\Theta\Delta\Theta + \mathbf{I}$. This equation defines the stretch in the position-gradient vectors in the initial configuration as the result of the thermal expansion as

$$\chi_{sk} = |(\mathbf{r}_{X_k})_o| = \sqrt{\left(\mathbf{r}_{X_k}^T\mathbf{r}_{X_k}\right)_o} = 1 + \alpha_{\Theta k}\Delta\Theta, \quad k = 1, 2, 3 \tag{10}$$

Because the thermal expansion does not produce shear and leads to only volumetric change, this equation can be used to determine the elements of the matrix of position-gradient vectors $\mathbf{J}_o^j$ that completely define the stress-free reference-configuration geometry when ANCF finite elements are used. Although the effect of the thermal expansion in the classical FE literature is introduced at the strain level, the preceding equation clearly shows the stretch of the position-gradient vectors as the result of the application of the thermal load, providing a more general interpretation of $\alpha_{\Theta k}\Delta\Theta(k = 1, 2, 3)$ as a position-gradient stretch coefficient.

Gradient-Based Thermal Analysis Approach

According to the definition of the gradient stretch $\chi_{sk}(k = 1, 2, 3)$ of Eq. (10), the change in the length of the gradient vector due to the thermal expansion is a function of the temperature change $\Delta\Theta$ as the result of assuming that the thermal expansion is related directly to the strains in the linear analysis. If the thermal expansions $\alpha_{\Theta k}\Delta\Theta(k = 1, 2, 3)$, are assumed to represent a dimensionless elongation, one can relate such an expansion directly to the stretch of the corresponding dimensionless nonunit position-gradient vector in the case of nonlinear geometry and analysis and write

$$\begin{aligned}(\mathbf{r}_{X_k})_{o+\Theta} &= d_{ok}(\hat{\mathbf{r}}_{X_k})_o + (\alpha_{\Theta k}\Delta\Theta)d_{ok}(\hat{\mathbf{r}}_{X_k})_o \\ &= d_{ok}(1 + \alpha_{\Theta k}\Delta\Theta)(\hat{\mathbf{r}}_{X_k})_o, \quad k = 1, 2, 3\end{aligned} \tag{11}$$

where $\hat{\mathbf{r}}_{X_k}$ is a unit vector along position-gradient vector $\mathbf{r}_{X_k}$; and d_{ok} is the length of gradient vector $\mathbf{r}_{X_k}$ before application of thermal load. Using the preceding equation, the stretch in the position-gradient vectors, which account for both effects of the reference-configuration geometry and thermal expansion, can be written

$$\chi_{gk} = |(\mathbf{r}_{X_k})_{o+\Theta}| = \sqrt{\left(\mathbf{r}_{X_k}^T\mathbf{r}_{X_k}\right)_{o+\Theta}} = d_{ok}(1 + \alpha_{\Theta k}\Delta\Theta), \quad k = 1, 2, 3 \tag{12}$$

The motivation for using the preceding equation is explained in the Appendix. The gradient-based approach discussed in this section does not use linearization or superposition assumptions in the definition of the Green–Lagrange strains. One can show that, when this approach is used, the normal components of the Green–Lagrange strains are defined before elastic strains develop as

$$\varepsilon_{kk} = [(d_{ok})^2(1 + \alpha_{\Theta k}\Delta\Theta)^2 - 1]/2, \quad k = 1, 2, 3 \tag{13}$$

This nonlinear definition is different from the linear strain definition used in the classical FE literature. The result of Eq. (12) also can be obtained using the second equation of Eq. (5),

$\mathbf{J}_{o+\Theta} = \mathbf{J}_{\Theta X}\mathbf{J}_o$, by defining the nonsingular thermal-gradient matrix $\mathbf{J}_{\Theta X}$ as $\mathbf{J}_{\Theta X} = \boldsymbol{\alpha}_\Theta \Delta\Theta + \mathbf{I}$, where $\boldsymbol{\alpha}_\Theta$ is a diagonal matrix that has the coefficients of thermal expansion $\alpha_{\Theta k}(k = 1, 2, 3)$, as its diagonal elements.

ANCF Implementation

In the absolute nodal coordinate formulation, the FE displacement field is written $\mathbf{r}(\mathbf{x}, t) = \mathbf{S}(\mathbf{x})\mathbf{e}(t)$, where $\mathbf{r}$ is the global position vector of an arbitrary point on the element, $\mathbf{S}$ is the element shape function matrix, $\mathbf{e}$ is the vector of element coordinates, and t is time (Shabana 2018). Because the vector of element nodal coordinates $\mathbf{e}$ includes position and position-gradient coordinates, the ANCF displacement field can describe arbitrarily large displacements without the need for introducing finite rotations which are not commutative and may lack physical interpretations (Shabana and Ling 2019). In the case of fully parameterized ANCF finite elements, the vector of coordinates at a given node k can be written in the spatial analysis as $\mathbf{e}^k = [\,\mathbf{r}^{kT} \quad \mathbf{r}_{x_1}^{kT} \quad \mathbf{r}_{x_2}^{kT} \quad \mathbf{r}_{x_3}^{kT}\,]^T$, where $k = 1, 2, \ldots, n_n$, where n_n is the number of nodes of the element. The vectors $\mathbf{r}_{x_1}^k$, $\mathbf{r}_{x_2}^k$, and $\mathbf{r}_{x_3}^k$ are position-gradient vectors that have unique geometric meaning as tangent to the FE coordinate lines x_1, x_2, and x_3. This geometric meaning is not shared by the displacement-gradient vectors, which are not tangent to the FE coordinate lines, as is discussed in the literature (Shabana 2015). Therefore, at a given node, the complete matrix of position-gradient vectors can be formulated to allow for conveniently describing the reference-configuration geometry as well as to account for the effect of thermal loads.

Background

In general, if the effect of the thermal load is not considered, the matrix $\mathbf{J}_o$ of position-gradient vectors in the reference configuration can be used to define the reference configuration geometry and perform local shape manipulation by changing the length and orientation of the position-gradient vectors at the nodes. This matrix of position-gradient vector in the current configuration, defined by differentiation with respect to the reference coordinates $\mathbf{X}$, can be written $\mathbf{J} = \partial\mathbf{r}/\partial\mathbf{X} = \mathbf{J}_e\mathbf{J}_o^{-1}$, where, $\mathbf{J}_e = \partial\mathbf{r}/\partial\mathbf{x}$ and $\mathbf{J}_o = \partial\mathbf{X}/\partial\mathbf{x}$. Because the reference configuration is assumed to be stress-free, the elastic Green–Lagrange strain tensor is zero before displacement regardless of the shape of the body. The Green–Lagrange strain tensor can be written $\boldsymbol{\varepsilon} = (\mathbf{J}^T\mathbf{J} - \mathbf{I})/2 = (\mathbf{J}_o^{-1^T}(\mathbf{J}_e^T\mathbf{J}_e)\mathbf{J}_o^{-1} - \mathbf{I})/2$. Before displacement, $\mathbf{J}_e = \mathbf{I}$, and therefore, $\boldsymbol{\varepsilon}$ is identically zero regardless of the geometry of the body which is defined by the nonsingular matrix $\mathbf{J}_o$. The matrix $\mathbf{J}_o$ can be formulated conveniently because the ANCF displacement field can always be written $\mathbf{r}(\mathbf{x}, t) = \mathbf{S}(\mathbf{x})(\mathbf{e}_o + \mathbf{e}_d)$, where $\mathbf{e}_o$ and $\mathbf{e}_d$ are, respectively, the vector of element coordinates in the reference configuration and the vector of displacement coordinates. Using the equation, $\mathbf{r}_o(\mathbf{x}) = \mathbf{S}(\mathbf{x})\mathbf{e}_o$, the matrix $\mathbf{J}_o$ can be formulated at a preprocessing stage before the start of the dynamic simulation. When the elastic forces are computed at the integration points, $\mathbf{J}_o$ is used in the definition of the Green–Lagrange strain tensor to ensure that the initial reference-configuration geometry has no effect on the computations of the elastic strains and stress forces. This procedure does not employ additive strain decompositions and is based mainly on the multiplicative decomposition of the matrix of position-gradient vector $\mathbf{J}$ as $\mathbf{J} = \partial\mathbf{r}/\partial\mathbf{X} = \mathbf{J}_e\mathbf{J}_o^{-1}$.

Generalization to Thermal Analysis

A similar procedure can be used in the case of thermal load. In this procedure, the additive strain decomposition is not used in order to ensure accurate description of the reference-configuration geometry and properly account for the effect of the thermal load. The procedure can be demonstrated using Eqs. (4) and (5) in the case of constant temperature. It was shown that in the case of constant temperature, one can write $d\mathbf{r} = (\partial\mathbf{r}/\partial\mathbf{X}_\Theta)d\mathbf{X}_\Theta = \mathbf{J}\mathbf{J}_{o+\Theta}d\mathbf{x}$, where $\mathbf{J} = \partial\mathbf{r}/\mathbf{X}_\Theta$ and $\mathbf{J}_{o+\Theta} = \mathbf{J}_{\Theta X}\mathbf{J}_o$. Because $d\mathbf{r}$ also can be written $d\mathbf{r} = (\partial\mathbf{r}/\partial\mathbf{x})d\mathbf{x} = \mathbf{J}_e d\mathbf{x} = \mathbf{J}\mathbf{J}_{o+\Theta}d\mathbf{x}$, one can write $\mathbf{J} = \mathbf{J}_e\mathbf{J}_{o+\Theta}^{-1}$. Substituting $\mathbf{J}$ in the Green–Lagrange strain tensor $\boldsymbol{\varepsilon}$ obtains

$$\boldsymbol{\varepsilon} = (\mathbf{J}^T\mathbf{J} - \mathbf{I})/2 = (\mathbf{J}_{o+\Theta}^{-1^T}(\mathbf{J}_e^T\mathbf{J}_e)\mathbf{J}_{o+\Theta}^{-1} - \mathbf{I})/2 \tag{14}$$

It is clear from this equation that, before displacement, if $\mathbf{J}_e = \mathbf{I}$, the Green–Lagrange strain tensor is identically zero. The matrix $\mathbf{J}_{o+\Theta}$ which accounts for both the reference-configuration geometry and the volumetric change due to the thermal load can be formulated conveniently using the ANCF equation $\mathbf{r}_{o+\Theta}(\mathbf{x}) = \mathbf{S}(\mathbf{x})\mathbf{e}_{o+\Theta}$, where the vector $\mathbf{e}_{o+\Theta}$ has the position-gradient vectors that properly account for the reference-configuration geometry as well as the effect of the thermal load. This can be accomplished using the stretch coefficients given by Eq. (12) as $\chi_{gk} = |(\mathbf{r}_{X_k})_{o+\Theta}| = d_{ok}(1 + \alpha_{\Theta k}\Delta\Theta)$, where $k = 1, 2, 3$, which ensure that the orientations of the gradient vectors are not affected by the application of the thermal load, which produces only fiber stretch and no shear.

Varying Temperature

In the case of varying temperatures, a similar procedure can be used using the definitions given by Eqs. (1)–(3). In this case, $\mathbf{J} = \mathbf{J}_{r\Theta}$ and $d\mathbf{r} = \mathbf{J}_e d\mathbf{x} = \mathbf{J}\mathbf{J}_o d\mathbf{x} = \mathbf{J}[\mathbf{J}_{\Theta X}\mathbf{J}_o]d\mathbf{x} = \mathbf{J}\mathbf{J}_{o+\Theta}d\mathbf{x}$, where $\mathbf{J}_{r\Theta} = \partial\mathbf{r}/\partial\mathbf{X}_\Theta$, $\mathbf{J}_{\Theta X} = \partial\mathbf{X}_\Theta/\partial\mathbf{X}$, $\mathbf{J}_o = \mathbf{J}_{Xx} = \partial\mathbf{X}/\partial\mathbf{x}$, and $\mathbf{J}_{o+\Theta} = \mathbf{J}_{\Theta X}\mathbf{J}_o$. As previously discussed, $\mathbf{J}_{\Theta X} = \boldsymbol{\alpha}_\Theta\Delta\Theta + \mathbf{I}$. In the case of varying temperature, $\Delta\Theta = \Delta\Theta(\mathbf{x}, t)$. By accounting for the change in the temperature profile and following the same procedure previously outlined in this section, one can show that the thermal load produces zero stresses. In this case, the matrix $\mathbf{J}_{\Theta X}$ must be updated properly at the integration points during the dynamic simulation.

ANCF Beam Element

This section uses a planar ANCF shear-deformable beam as an example to demonstrate the implementation and use of the approach discussed in this paper. The procedure described in this paper, however, is applicable to all ANCF fully parameterized elements.

Element Displacement Field

A two-dimensional ANCF shear deformable beam element has two nodes. Each node k of element j has six degrees of freedom: two translational coordinates $\mathbf{r}^{jk}$ and four gradient coordinates defined by the two vectors $\mathbf{r}_{x_1}^{jk}$ and $\mathbf{r}_{x_2}^{jk}$, where $k = 1, 2$. The vector of nodal coordinates at each node is defined as $\mathbf{e}^{jk} = [\,(\mathbf{r}^{jk})^T \quad (\mathbf{r}_{x_1}^{jk})^T \quad (\mathbf{r}_{x_2}^{jk})^T\,]^T$, and therefore, the element has 12 coordinates. The position vector of a point on the element can be written $\mathbf{r}^j = \mathbf{S}^j\mathbf{e}^j$, where $\mathbf{S}^j$ and $\mathbf{e}^j$ are, respectively, the element shape function matrix and the vector of nodal coordinates, which can be written

$$\mathbf{S}^j = [\, s_1\mathbf{I} \quad s_2\mathbf{I} \quad s_3\mathbf{I} \quad s_4\mathbf{I} \quad s_5\mathbf{I} \quad s_6\mathbf{I} \,]$$
$$\mathbf{e}^j = [\, (\mathbf{e}^{j1})^T \quad (\mathbf{e}^{j2})^T \,]^T \tag{15}$$

where $\mathbf{I}$ is a 2×2 identity matrix and the shape functions $s_i (i = 1, 2, \ldots, 6)$ are

$$s_1 = 1 - 3\xi^2 + 2\xi^3, \quad s_2 = l(\xi - 2\xi^2 + \xi^3), \quad s_3 = l(\eta - \xi\eta)$$
$$s_4 = 3\xi^2 - 2\xi^3, \quad s_5 = l(-\xi^2 + \xi^3), \quad s_6 = l\xi\eta \tag{16}$$

where $\xi = x_1^j/l$; $\eta = x_2^j/l$, and l is the element length. The vectors of position gradients of an element j are

$$\mathbf{r}_{x_1}^j = \frac{\partial \mathbf{r}^j}{\partial x_1} = s_{1,1}\mathbf{r}^{j1} + s_{2,1}\mathbf{r}_{x_1}^{j1} + s_{3,1}\mathbf{r}_{x_2}^{j1} + s_{4,1}\mathbf{r}^{j2} + s_{5,1}\mathbf{r}_{x_1}^{j2} + s_{6,1}\mathbf{r}_{x_2}^{j2}$$
$$\mathbf{r}_{x_2}^j = \frac{\partial \mathbf{r}^j}{\partial x_2} = s_{3,2}\mathbf{r}_{x_2}^{j1} + s_{6,2}\mathbf{r}_{x_2}^{j2} \tag{17}$$

where $s_{m,n} = \partial s_m/\partial x_n$, where $m = 1, 2, \ldots, 6$, and $n = 1, 2$; and

$$s_{1,1} = 6(-\xi + \xi^2)/l, \qquad s_{2,1} = (1 - 4\xi + 3\xi^2),$$
$$s_{3,1} = -\eta, \qquad s_{4,1} = 6(\xi - \xi^2)/l \qquad s_{5,1} = (-2\xi + 3\xi^2),$$
$$s_{6,1} = \eta, \qquad s_{3,2} = (1 - \xi), \qquad s_{6,2} = \xi \tag{18}$$

Thermal Expansion

Thermal expansion has an effect on the total strains as well as on the position gradients which are used as ANCF nodal coordinates. The position vector of an arbitrary point on the ANCF element can be written before the load application as $\mathbf{r}_{o+\Theta}^j = \mathbf{S}^j(\mathbf{e}_o^j + \mathbf{e}_\Theta^j) = \mathbf{S}^j\mathbf{e}_{o+\Theta}^j$, where the vector $\mathbf{e}_\Theta^j$ accounts for the change in the element nodal coordinates due to the thermal expansion. For example, if the reference configuration before the application of the thermal load is assumed to be the straight configuration ($\mathbf{X} = \mathbf{x}$), the vector of nodal coordinates $\mathbf{e}^j$ before displacement and application of the thermal load can be written $\mathbf{e}_o^j = [\,0 \;\; 0 \;\; 1 \;\; 0 \;\; 0 \;\; 1 \;\; l \;\; 0 \;\; 1 \;\; 0 \;\; 0 \;\; 1\,]^T$. In this case, the change in the longitudinal nodal gradient vector $\Delta\mathbf{r}_{x_1}^{jk}$ in $\mathbf{e}_\Theta^j$ due to the thermal expansion is $\Delta\mathbf{r}_{x_1}^{jk} = [\,\alpha_\Theta\Delta\Theta \quad 0\,]^T$, where $k = 1, 2$, α_Θ is the coefficient of thermal expansion, and $\Delta\Theta$ is the temperature change. Integrating $\Delta\mathbf{r}_{x_1}^{jk} = [\,\alpha_\Theta\Delta\Theta \quad 0\,]^T$ $(k = 1, 2)$ obtains the change in the nodal position due to the thermal expansion as $\int_0^l \alpha_\Theta\Delta\Theta dx_1 = \alpha_\Theta l\Delta\Theta$. Using a similar procedure for the lateral gradient vector $\mathbf{r}_{x_2}^{jk}$, $k = 1, 2$, one can write $\mathbf{e}_{o+\Theta}^j = [\,(\mathbf{e}_{o+\Theta}^{j1})^T \quad (\mathbf{e}_{o+\Theta}^{j2})^T\,]^T$, where

$$\mathbf{e}_{o+\Theta}^{j1} = [\,0 \quad 0 \quad 1 + \alpha_\Theta\Delta\Theta \quad 0 \quad 0 \quad 1 + \alpha_\Theta\Delta\Theta\,]^T$$
$$\mathbf{e}_{o+\Theta}^{j2} = [\,l(1 + \alpha_\Theta\Delta\Theta) \quad 0 \quad 1 + \alpha_\Theta\Delta\Theta \quad 0 \quad 0 \quad 1 + \alpha_\Theta\Delta\Theta\,]^T \tag{19}$$

Using the vector $\mathbf{e}_{o+\Theta}^j$ in the element displacement field $\mathbf{r}^j = \mathbf{S}^j\mathbf{e}_{o+\Theta}^j$, one can show that the position vector of an arbitrary point on the beam can be written as $\mathbf{r}^j = [\,r_1 \quad r_2\,]^T$, where $r_1 = l\xi(1 + \alpha_\Theta\Delta\Theta)$ and $r_2 = l\eta(1 + \alpha_\Theta\Delta\Theta)$, and $\mathbf{X}_\Theta = [\,X_{\Theta 1} \quad X_{\Theta 2}\,]^T$, where $X_{\Theta 1} = (l\xi)\alpha_\Theta\Delta\Theta$ and $X_{\Theta 2} = (l\eta)\alpha_\Theta\Delta\Theta$. The position-vector gradients can be written $\mathbf{r}_{x_1}^j = [\,1 + \alpha_\Theta\Delta\Theta \quad 0\,]^T$ and $\mathbf{r}_{x_2}^j = [\,0 \quad 1 + \alpha_\Theta\Delta\Theta\,]^T$. The matrix of position-vector gradients due to the temperature effect in the straight-element configuration can be defined as

$$\mathbf{J}_{\Theta x}^j = \begin{bmatrix} 1 + \alpha_\Theta\Delta\Theta & 0 \\ 0 & 1 + \alpha_\Theta\Delta\Theta \end{bmatrix} \tag{20}$$

This equation shows a homogeneous displacement that represents a uniform gradient thermal expansion distribution within the ANCF element. This matrix of position-gradient vectors has the determinant $J_{\Theta x}^j = (1 + \alpha_\Theta\Delta\Theta)^2$. The relationship between the volumes in the thermally expanded element and straight-element configurations at an arbitrary material point can be written $dV_\Theta^j = J_{\Theta x}^j dV^j$, where V^j and V_Θ^j are the volumes of element in the straight and thermally expanded configurations, respectively. If $\mathbf{X}_\Theta^j$ is considered as the reference configuration, one can define the volume in the current configuration as $dv^j = J^j dV_\Theta^j = J^j J_{\Theta X}^j dV_o^j = J^j J_{\Theta X}^j J_{Xx}^j dV^j$, where $J^j = |\mathbf{J}^j|$ is the determinant of the matrix of position-vector gradients $\mathbf{J}^j = \partial\mathbf{r}^j/\partial\mathbf{X}_\Theta^j$, $J_{\Theta X}^j = |\partial\mathbf{X}_\Theta^j/\partial\mathbf{X}^j|$, and $J_{Xx}^j = |\partial\mathbf{X}^j/\partial\mathbf{x}^j|$. The four configurations used in this description are shown in Fig. 1, where that V, V_o, V_Θ, and v are the volumes in the straight, intermediate reference with no thermal expansion, thermally expanded reference, and current deformed configurations, respectively, and $\mathbf{x}$, $\mathbf{X}$, $\mathbf{X}_\Theta$, and $\mathbf{r}$ are the associated position vectors in these four configurations, as previously mentioned. In the problem considered in this investigation, the integration with respect to the thermally expanded reference domain $\mathbf{X}_\Theta$ can be conveted to integration with respect to the straight element domain $\mathbf{x}$. When performing the integration with respect to the straight configuration $\mathbf{x}$, the dimensions of the straight element should be used. The expansion effect on the integration is accounted for using the determinant $|\mathbf{J}_{\Theta X}^j\mathbf{J}_{Xx}^j| = |\mathbf{J}_{\Theta x}^j|$.

Numerical Results

This section presents numerical results to demonstrate the use and implementation of the approach described in this paper. A thermal load was applied to the two-dimensional ANCF shear-deformable beam element at a preprocessing stage to obtain the coordinates in the thermally expanded configuration $\mathbf{X}_\Theta$. The beam length was assumed to be $l = 1$ m, and the cross-section dimension is $A = 0.3 \times 0.3$ m^2. The beam was subjected to a constant thermal load, and the coefficient of thermal expansion and temperature change were assumed to be $\alpha_\Theta = 0.002(1/°\text{C})$ and $\Delta\Theta = 200°\text{C}$, respectively.

Fig. 2 compares the original shape and thermally expanded shape of a two-dimensional ANCF straight beam. It was assumed that the beam was fully clamped at its first end. The figure shows the stretch of the cross-section and the change in the nodal positions as the result of the thermal expansion. Fig. 3 shows the change of the norm of the gradient vector $\mathbf{r}_{x_1}$ with respect to the beam length. Because of the symmetry, similar behavior was observed with the norm of the gradient vector $\mathbf{r}_{x_2}$.The results obtained demonstrate

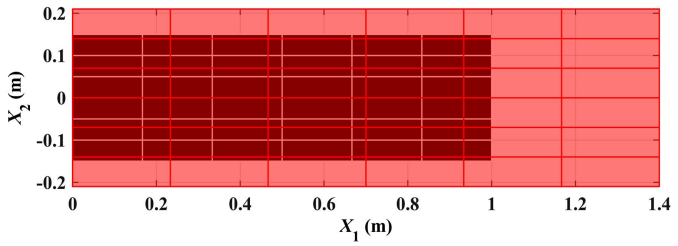

Fig. 2. Effect of thermal expansion on the straight beam.

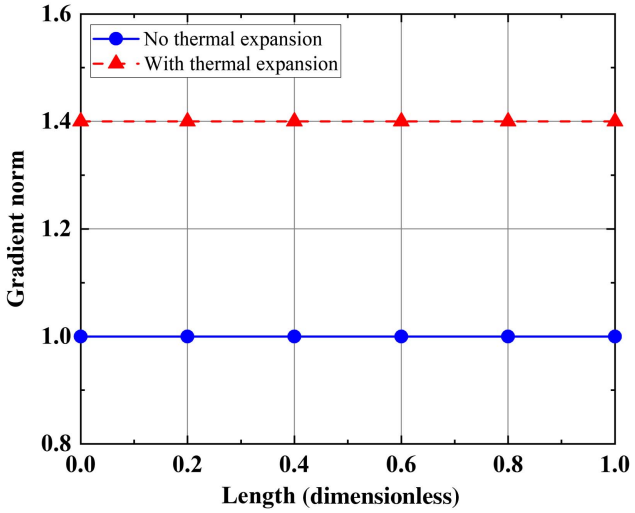

Fig. 3. Norm of the gradient vector $\mathbf{r}_{x_1}^j$.

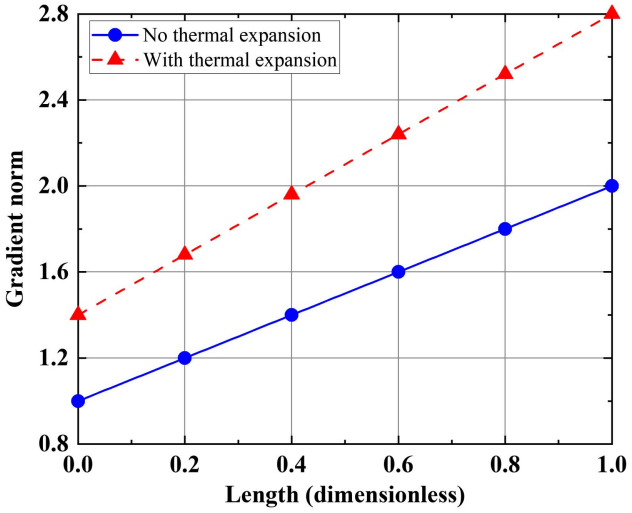

Fig. 5. Norm of the gradient vector $\mathbf{r}_{x_2}^j$.

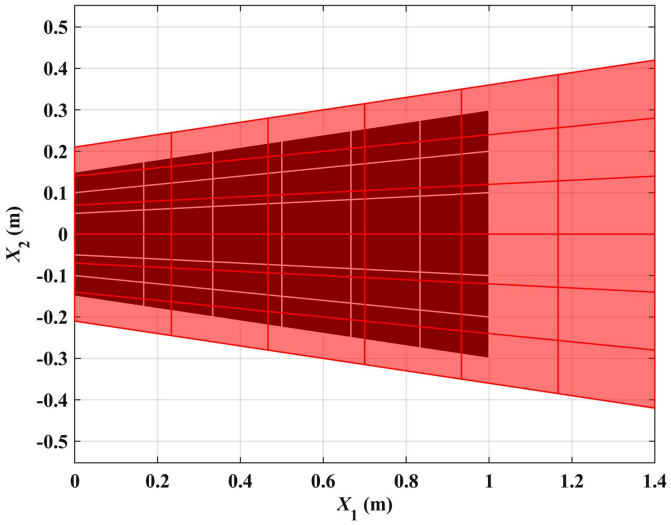

Fig. 4. Effect of thermal expansion on the tapered beam.

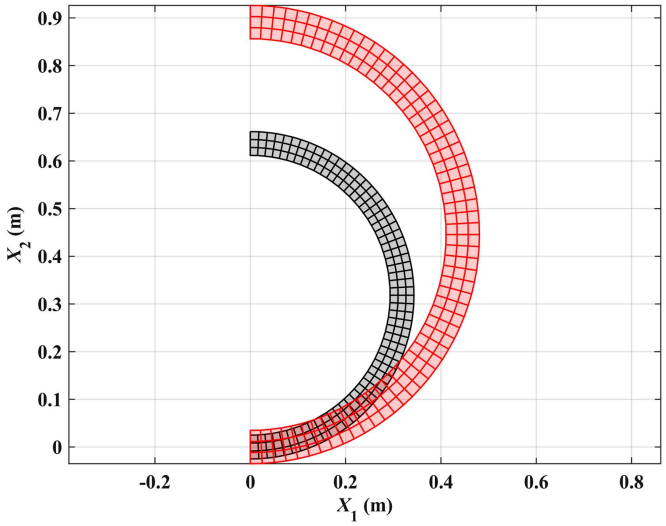

Fig. 6. Effect of thermal expansion on the initially curved beam.

the uniform gradient thermal expansion distribution obtained within the ANCF element.

Fig. 4 compares the original shape and thermally expanded shape of a two-dimensional ANCF tapered beam, in which the initial vector of nodal coordinates $\mathbf{e}_o^j$ before the application of the thermal load was defined as $\mathbf{e}_o^j = [0 \;\; 0 \;\; 1 \;\; 0 \;\; 0 \;\; 1 \;\; l \;\; 0 \;\; 1 \;\; 0 \;\; 0 \;\; 2]^T$. Using Eq. (12), the lateral gradients at the nodal point considering the thermal expansion can be calculated as $\mathbf{r}_{x_2}^{j1} = [0 \;\; 1.4]^T$ and $\mathbf{r}_{x_2}^{j2} = [0 \;\; 2.8]^T$. The figure shows the cross-section stretch as well as the displacements within the tapered beam as the result of the thermal expansion. The results obtained showed that the norm of $\mathbf{r}_{x_1}^j$ is the same as that reported in Fig. 3. The norm of $\mathbf{r}_{x_2}^j$ has a linear distribution in the case of the tapered beam (Fig. 5).

A third example is the curved beam in Fig. 6. The beam had the geometry of a half circle. The circular beam reference-configuration geometry was obtained from a straight beam with length $l = 1$ m and cross-section area $A = 0.05 \times 0.05$ m^2. The radius of the circle in the reference configuration before the application of the thermal load was $r = l/\pi$ m. The beam was divided into 30 ANCF two-dimensional fully parameterized ANCF beam elements. The material properties were assumed to be the same as used in the preceding example. The beam was subjected to a temperature increase of $\Delta\Theta = 200$°C, and the coefficient of thermal expansion was $\alpha_\Theta = 0.002(1/°C)$. Fig. 6 shows the response of the beam to the thermal load.

Numerical Solutions

To show the effect of the thermal expansion on the solution, a simple cantilever beam example was considered. The beam was subjected to an axial constant load force $P = 1.0 \times 10^3$ N in the positive x_1-direction, and the gravity effect was neglected. The dimensions of the beam were the same as the those of the straight beam previously considered in this section. The beam was assumed to be made of a soft material governed by a linear elastic model. The modulus of elasticity and Poisson's ratio were assumed to be $E = 1.2 \times 10^6$ N/m^2 and $\mu = 0.3$, respectively. The density of the beam was $\rho = 1{,}500$ kg/m^3 (Trivedi et al. 2008). For the soft materials, such as polyethylene or paraffin, the general coefficient

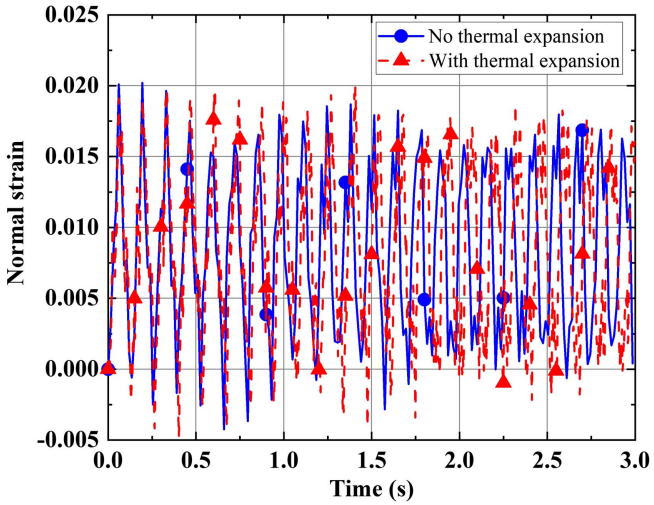

Fig. 7. Axial normal-strain change at the midpoint.

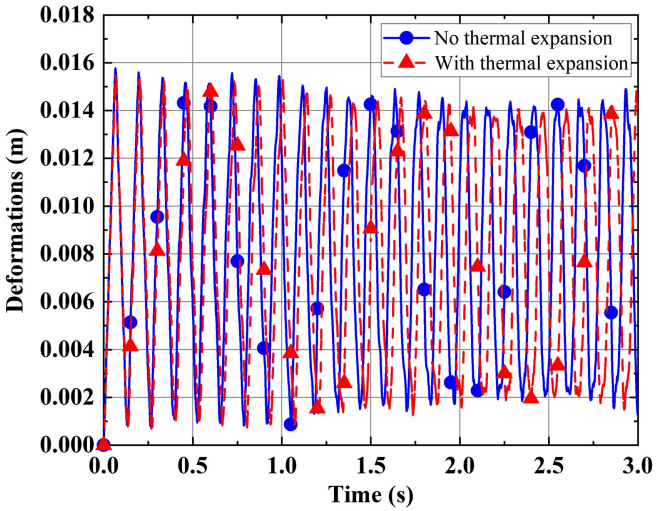

Fig. 9. Free-end deformation of soft material.

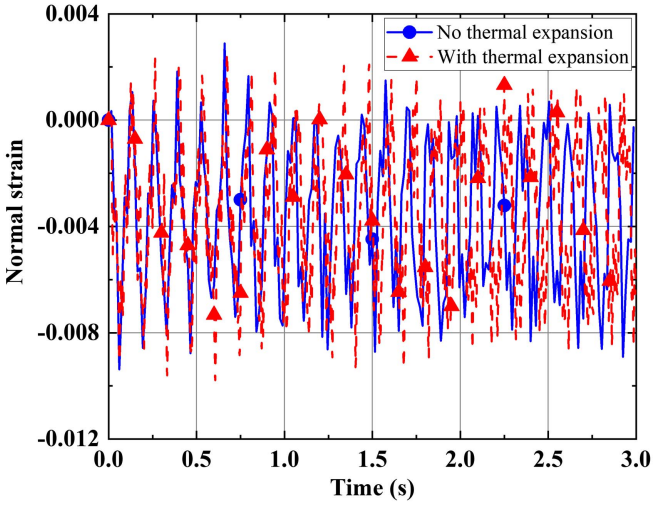

Fig. 8. Transverse normal-strain change at the midpoint.

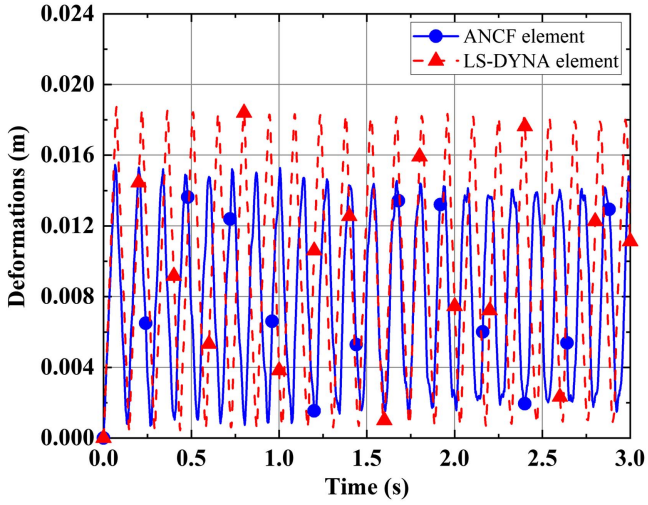

Fig. 10. Free-end deformation of soft material in the case of thermal expansion.

of thermal expansion was assumed to be $\alpha_\Theta = 0.0001(1/°C)$ (Engineering ToolBox 2003). The temperature change was assumed to be $\Delta\Theta = 200°C$. The general continuum mechanics approach, based on the plane-strain assumption, was used to formulate the elastic forces, and the total simulation time was assumed to be $t = 3$ s. The cantilever beam was modeled using 10 ANCF beam elements, and the effect of damping is neglected. Figs. 7 and 8 show the change in the normal elastic strains with respect to the initial normal strains in the axial and transverse directions at the midpoint of the beam. The change of the normal strains was found to increase as the result of the application of the thermal load, which was accounted for by changing the strains at the nodal points (Logan 2017). Fig. 9 shows the converged solution of the deformation of the beam free end along the axial direction.

The ANCF beam results obtained in this example were verified by comparison with the commercial software LS-DYNA version 4.5.23. The cantilever beam was modeled by a two-node Belytschko–Schwer beam element with full cross-section integration. The number of Gaussian integration points on the cross section was 3×3. Furthermore, an explicit integration method was used in both the ANCF and the LS-DYNA solutions to avoid the numerical damping in implicit solvers. In the LS-DYNA solution, the verification procedure involved two steps. The first step was to perform the preload initialization analysis with the thermal load. The thermal load was implemented using the function MAT_ADD_THERMAL_EXPANSION to set the linear thermal expansion coefficients, and the function LOAD_THERMAL_CURVE to set the constant temperature change. In this step, only thermal load was imposed in order to reach the thermally expanded equilibrium configuration. LS-DYNA produced an output dynain file that contained the nodal stress information of the thermally expanded beam using the selection SPRINGBACK_LSDYNA of the INTERFACE menu. The second step was to perform a dynamic analysis with the mechanical load. The thermally expanded cantilever configuration was used an input by selecting INCLUDE from the dynain file created in the first step. The load in the model contained only the mechanical load (LS-DYNA 2008). Fig. 10 shows the converged deformation results with the thermal load using 30 elements obtained from LS-DYNA, and the converged deformation result obtained using ANCF solution. The frequency of the deformation was similar in both cases, but the LS-DYNA results had higher

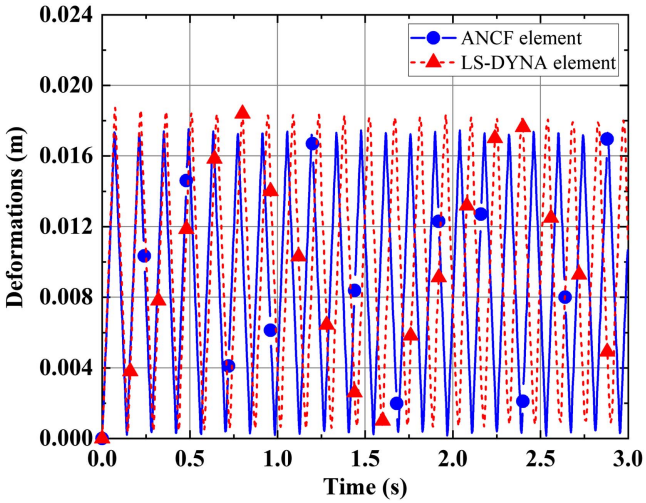

Fig. 11. Free-end deformation with $\mu = 0$ Poisson's ratio in the case of thermal expansion.

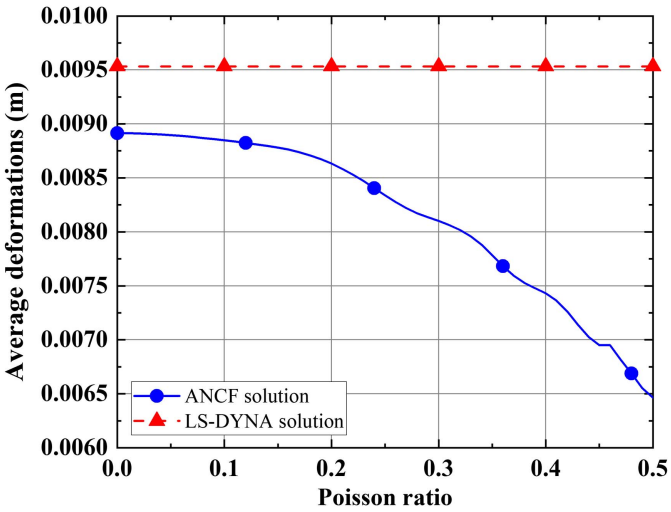

Fig. 12. Average free-end deformation in the case of thermal expansion.

amplitudes than the ANCF results. The two solutions had better agreement in the case of zero Poisson's ratio (Fig. 11). This result was expected because the ANCF beam element is a higher-order element that has more deformation modes, and consequently, geometric stiffening is an issue. Furthermore, there were significant differences between the assumed displacement fields of ANCF elements and LS-DYNA elements. Fig. 12 shows the variation of the average amplitudes of the free-end deformation as function of Poisson's ratio. The results in Fig. 12 demonstrate that the LS-DYNA beam element is not sensitive to the change in Poisson's ratio because of the assumption of a constant cross section. Fig. 13 presents the deformations predicted using the ANCF linear Hookean and nonlinear compressible neo-Hookean models when the thermal load was applied for different values of the Poisson's ratio μ. The results in Fig. 13 show that the nonlinear material model can have a larger amplitude.

In the case of the soft materials, the literature reports that temperature can have a softening effect, and the material stiffness can be controlled by embedding thermally softened structures, such as

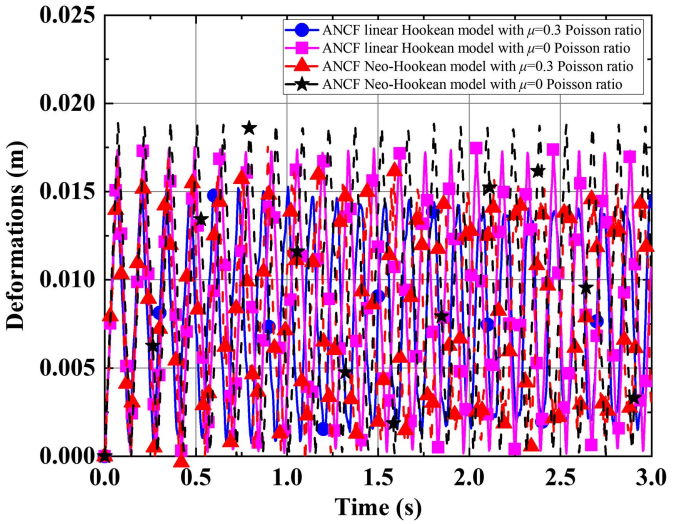

Fig. 13. Linear and nonlinear material models.

wax (Karbhari 2007; Rus and Tolley 2015). For fluid, the literature reports that thermal softening can have a significant effect on the viscosity of a fluid whose motion is governed by shear forces (Bair 2019).

Discussion

The results in Fig. 10 show differences between the LS-DYNA and ANCF solutions. These differences in general are attributed to the use of fundamentally different displacement fields. The ANCF displacement field leads to coupled deformation modes which lead to a slight increase in the stiffness, the effect of which becomes more significant as the Poisson's ratio increases, as discussed in the literature. Furthermore, the two different types of elements use different coordinates, and the boundary conditions at the fixed end are different. In the ANCF model, fully clamped end conditions are used to eliminate the translations, rotation, and the three strain modes. The ANCF element also is allowed to stretch in the transverse direction and such mode of deformation absorbs energy that otherwise would contribute to a larger axial displacement. Therefore, the energy distribution among different deformation modes is different in the case of the ANCF elements. In the case of the LS-DYNA element, the cross section does not deform, and consequently, no energy is consumed in the stretch of the cross section. It is clear, however, that these differences decrease as the Poisson's ratio decreases (Fig. 11). It also is clear that the phase shift at the beginning of the simulation is insignificant (Figs. 10 and 11). In addition to the fact that the two elements have different displacement fields, the solution procedures used for the two models are different. The ANCF model uses a nonincremental solution procedure. Furthermore, the numerical integration methods used for the two models are different, and as the simulation time increases, differences between the two solutions are expected. The relatively stiffer behavior observed when using ANCF finite elements should not be attributed to locking; it was found that this stiffer behavior is the result of using the plane-strain assumption. Fig. 14 compares the ANCF solutions using plane-strain and plane-stress assumptions. It is clear that the ANCF solution with the plane-stress assumption is closer to the LS-DYNA solution. The results in Fig. 14 shed light on the importance of considering the constitutive models when performing comparative and verification studies.

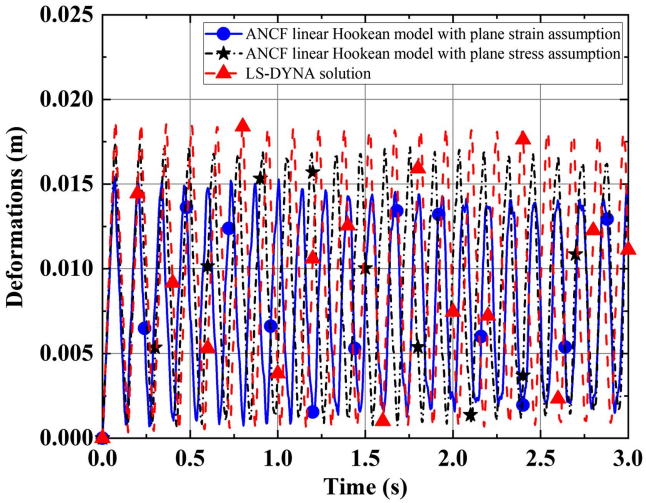

Fig. 14. Free-end deformation of soft material in the case of thermal expansion.

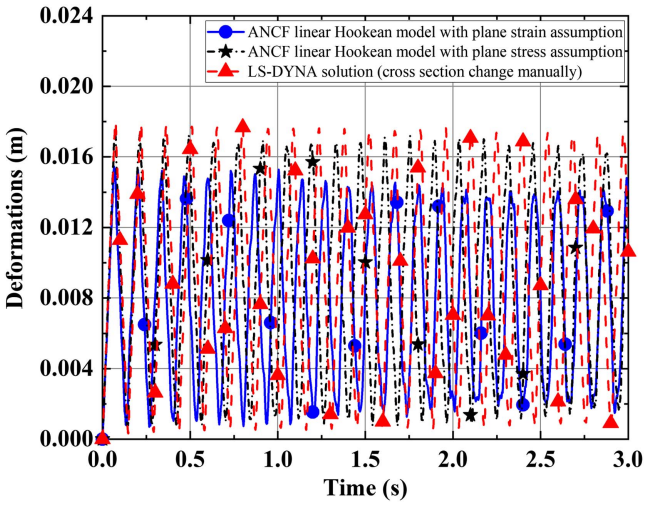

Fig. 15. Free-end deformation of soft material in the case of thermal expansion.

Some commercial FE software provides an option to use an ad hoc approach to account for the stretch of the cross section. For the LS-DYNA beam element used in this paper, the cross section was assumed to be rigid and could not be stretched. If an ad hoc approach is used to allow for the cross-section stretch, the LS-DYNA free-end deformation in Fig. 15 decreases, and the solution converges to the ANCF solution. This demonstrates the limitations of the LS-DYNA Belytschko element, and also demonstrates that the stiff behavior of the ANCF element should not be interpreted as locking.

The material used in this paper was assumed to be polyethylene, which has a yield stress in the range 26–33 MPa (Beer et al. 2009). For the temperature change of 200°C considered in this investigation, the maximum values of the axial and transverse strains were approximately 0.02 and 0.008, respectively. Therefore, the maximum axial and transverse stresses were in the range of 0.024 and 0.0096 MPa, respectively. These stress values were far below the yield stress of polyethylene material, and therefore the assumption of elastic behavior used in this study was justified.

Summary and Conclusions

This investigation proposes a new computational procedure that accounts for the reference-configuration geometry for the solution of the thermoelasticity problem (Lubarda 2004; Vujosevic and Lubarda 2002; Darijani and Naghdabadi 2013). This approach alleviates the limitations of the classical thermal-analysis approaches that are based on the strain additive decomposition. Existing thermal-analysis formulations do not properly capture the effect of complex stress-free reference-configuration geometries, restrict the algorithms to small-deformation problems, and lead to simplified linearized expression for the Green–Lagrange strain tensor. Using ANCF displacement fields which employ position-gradient vectors as nodal coordinates, a new ANCF gradient-based approach is proposed. This approach employs a multiplicative decomposition of the matrix of position-gradient vectors into two position-gradient matrices; one matrix is associated with the reference-configuration geometry before the application of the thermal load, and the other matrix accounts for the volumetric change due to the change in temperature. A numerical study demonstrated the use of the gradient-based approach in the thermal analysis.

In engineering systems, the reference-geometry of components is not always simple. For such systems, the change in temperature leads to stress-free thermal expansion of this reference-configuration geometry which must be accounted for accurately to properly capture the thermal effect. The additive strain decomposition in the thermal analysis involves approximation based on neglecting geometric nonlinearities. The approach presented in this study relaxes these assumptions by developing a new ANCF multiplicative-decomposition procedure that properly accounts for geometric nonlinearities. Furthermore, this approach allows for the use of nonlinear constitutive models and nonlinear strain-displacement relationships, as demonstrated in this paper. The approach presented in this paper also is fundamentally different from the thermal-expansion approach for the small deformation analysis based on the floating frame of reference (FFR) formulation (Ukani et al. 1988; Shabana 1986).

Appendix. Interpretation of Coefficient of Thermal Expansion

This Appendix explains the motivation for using the gradient-based thermal-expansion approach employed in this investigation. In practice, the coefficients of thermal expansion can be measured along directions. These directions can be defined conveniently using the position-gradient vectors which are tangents to the material fibers. This study defined the thermal expansion using the norm of the position-gradient vectors $\chi_{gk} = |(\mathbf{r}_{X_k})_{o+\Theta}|$ by the equation

$$\chi_{gk} = |(\mathbf{r}_{X_k})_{o+\Theta}| = \sqrt{(\mathbf{r}_{X_k}^T \mathbf{r}_{X_k})_{o+\Theta}} = d_{ok}(1+\alpha_{\Theta k}\Delta\Theta), \quad k = 1,2,3 \tag{21}$$

For example, in planar problems, the thermal expansion in the longitudinal and transverse directions can be conveniently measured along the position-gradient vectors $\mathbf{r}_{X_k}(k = 1, 2)$. It is important, however, to distinguish between this interpretation and an interpretation based on a definition of an arbitrary line element.

To explain the differences between the two interpretations, for simplicity, it is assumed that the straight configuration $\mathbf{x}$ is the same as the reference configuration $\mathbf{X}$. The length of the line element in the thermally expanded configuration $\mathbf{X}_\Theta$ is defined as $l_\Theta = \sqrt{d\mathbf{X}_\Theta^T d\mathbf{X}_\Theta}$, whereas the length in the straight configuration

can be written $l_o = \sqrt{d\mathbf{X}^T d\mathbf{X}}$. The change in the length of the line element due to the temperature change can be written $dl_\Theta = l_\Theta - l_o = (\alpha_\Theta \Delta\Theta) l_o$. Using this interpretation, one can write

$$\sqrt{d\mathbf{X}_\Theta^T d\mathbf{X}_\Theta} - \sqrt{d\mathbf{X}^T d\mathbf{X}} = \alpha_\Theta \Delta\Theta \sqrt{d\mathbf{X}^T d\mathbf{X}} \tag{22}$$

The relationship $d\mathbf{X}_\Theta = \mathbf{J}_{\Theta X} d\mathbf{X}$, where $\mathbf{J}_{\Theta X} = \partial \mathbf{X}_\Theta / \partial \mathbf{X}$, can be used to write the preceding equation as

$$\sqrt{d\mathbf{X}^T \mathbf{J}_{\Theta X}^T \mathbf{J}_{\Theta X} d\mathbf{X}} - \sqrt{d\mathbf{X}^T d\mathbf{X}} = \alpha_\Theta \Delta\Theta \sqrt{d\mathbf{X}^T d\mathbf{X}} \tag{23}$$

If the principal directions are assumed, the matrix $\mathbf{J}_{\Theta X}^T \mathbf{J}_{\Theta X}$ is diagonal and can be written

$$\mathbf{J}_{\Theta X}^T \mathbf{J}_{\Theta X} = \begin{bmatrix} \mathbf{r}_{X_{\Theta 1}}^T \mathbf{r}_{X_{\Theta 1}} & 0 & 0 \\ 0 & \mathbf{r}_{X_{\Theta 2}}^T \mathbf{r}_{X_{\Theta 2}} & 0 \\ 0 & 0 & \mathbf{r}_{X_{\Theta 3}}^T \mathbf{r}_{X_{\Theta 3}} \end{bmatrix} \tag{24}$$

Using the definition of the unit vector $\mathbf{n} = [\, n_1 \quad n_2 \quad n_3 \,]^T = d\mathbf{X}/l_o$ and Eq. (23)

$$\sqrt{\sum_{k=1}^{3} (\mathbf{r}_{X_{\Theta k}}^T \mathbf{r}_{X_{\Theta k}}) n_k^2} = (1 + \alpha_\Theta \Delta\Theta) \tag{25}$$

This equation demonstrates the difficulty of using the general formulation of the arbitrary line element as the basis for defining the coefficient of thermal expansion; this is true even if the principal directions can be identified and used as the measurement directions. This explains the motivation for using the norm of the position-gradient vectors as the basis for the definition of the thermal expansion. This gradient-based definition also is more consistent with the measurements made to define the coefficient of thermal expansion.

Data Availability Statement

Some or all data, models, or code that support the findings of this study are available from the corresponding author upon reasonable request.

Acknowledgments

This research was supported by the National Science Foundation (Project Nos. 1632302 and 1852510), and by China Postdoctoral Science Foundation (Project No. 2020M683601).

References

API (American Petroleum Institute). 2004. "Temperature and pressure volume correction factors for generalized crude oils, refined products, and lubricating oils." Chap. 11.1 in *Manual of petroleum measurement standards*. Washington, DC: API Publishing Services.

Bair, S. 2019. *High pressure rheology for quantitative elastohydrodynamics*. 2nd ed. 223–257. Amsterdam, Netherlands: Elsevier Science.

Beer, F., R. Johnston, J. Dewolf, and D. Mazurek. 2009. *Mechanics of materials*. New York: McGraw-Hill Companies.

Bonet, J., and R. D. Wood. 1997. *Nonlinear continuum mechanics for finite element analysis*. Cambridge, UK: Cambridge University Press.

Bower, A. F. 2009. *Applied mechanics of solids*. 1st ed. Boca Raton, FL: CRC Press.

Chang, C., Q. D. Nguyen, and H. P. Rønningsen. 1999. "Isothermal start-up of pipeline transporting waxy crude oil." *J. Non-Newtonian Fluid Mech.* 87 (2–3): 127–154. https://doi.org/10.1016/S0377-0257(99)00059-2.

Chen, Y., D. G. Zhang, and L. Li. 2019. "Dynamic analysis of rotating curved beams by using Absolute Nodal Coordinate Formulation based on radial point interpolation method." *J. Sound Vib.* 441: 63–83. https://doi.org/10.1016/j.jsv.2018.10.011.

Cook, R. D. 1981. *Concepts and applications of finite element analysis*. New York: Wiley.

Cui, Y.-Q., Z.-Q. Yu, and P. Lan. 2019. "A novel method of thermo-mechanical coupled analysis based on the unified description." *Mech. Mach. Theory* 134: 376–392. https://doi.org/10.1016/j.mechmachtheory.2019.01.001.

Darijani, H., and R. Naghdabadi. 2013. "Kinematics and kinetics modeling of thermoelastic continua based on the multiplicative decomposition of the deformation gradient." *Int. J. Eng. Sci.* 62: 56–69. https://doi.org/10.1016/j.ijengsci.2012.07.001.

Dmitrochenko, O. N., and D. Y. Pogorelov. 2003. "Generalization of plate finite elements for absolute nodal coordinate formulation." *Multibody Syst. Dyn.* 10 (1): 17–43. https://doi.org/10.1023/A:1024553708730.

Dorfman, A., and Z. Renner. 2009. "Conjugate problems in convective heat transfer: Review." *Math. Probl. Eng.* 2009: 927350. https://doi.org/10.1155/2009/927350.

Engineering ToolBox. 2003. "Coefficients of linear thermal expansion." Accessed Februrary 22, 2021. https://www.engineeringtoolbox.com/linear-expansion-coefficients-d_95.html.

Errara, M. P., and S. Chemin. 2013. "Optimal solutions of numerical interface conditions in fluid–structure thermal analysis." *J. Comput. Phys.* 245 (Jul): 431–455. https://doi.org/10.1016/j.jcp.2013.03.004.

Farin, G. 1999. *Curves and surfaces for CAGD: A practical guide*. 5th ed. San Francisco: Morgan Kaufmann.

Fotland, G., C. Haskins, and T. Rølvåg. 2019. "Trade study to select best alternative for cable and pulley simulation for cranes on offshore vessels." *Syst. Eng.* 23 (2): 177–188. https://doi.org/10.1002/sys.21503.

Gallier, J. 2011. *Geometric methods and applications: For computer science and engineering*. New York: Springer.

Goetz, A. 1970. *Introduction to differential geometry.* Upper Saddle River, NJ: Addison Wesley.

Helselhaus, A., T. Vogel, and H. Krain. 1992. "Coupling of 3D-Navier-Stokes external flow calculations and internal 3D-heat-conduction calculations for cooled turbine blades." In *Proc., AGARD Meeting on Heat Transfer and Cooling in Gas Turbines*, 40-1–40-9. Köln-Porz, Germany: AGARD.

Henshaw, W. D., and K. K. Chand. 2009. "A composite grid solver for conjugate heat transfer in fluid–structure systems." *J. Comput. Phys.* 228 (10): 3708–3741. https://doi.org/10.1016/j.jcp.2009.02.007.

Hewlett, J. 2019. "Methods for real-time simulation of systems of rigid and flexible bodies with unilateral contact and friction." Ph.D. thesis, Dept. of Mechanical Engineering, McGill Univ.

Hewlett, J., S. Arbatani, and J. Kovecses. 2020. "A fast and stable first-order method for simulation of flexible beams and cables." *Nonlinear Dyn.* 99 (2): 1211–1226. https://doi.org/10.1007/s11071-019-05347-1.

Htun, T. Z., H. Suzuki, and D. Garcia-Vallejo. 2020. "Dynamic modeling of a radially multilayered tether cable for a remotely-operated underwater vehicle (ROV) based on the absolute nodal coordinate formulation (ANCF)" *Mech. Mach. Theory* 153: 103961. https://doi.org/10.1016/j.mechmachtheory.2020.103961.

Karbhari, V. M., ed. 2007. "Fabrication, quality and service-life issues for composites in civil engineering." In Chap. 2 in *Durability of composites for civil structural applications*, 13–30. 1st ed. Lisle, IL: Woodhead.

Khan, I. M., and K. S. Anderson. 2013. "Divide-and-conquer-based large deformation formulations for multi-flexible body systems." In Vol. 7B of *Proc., ASME 9th Int. Conf. on Multibody Systems, Nonlinear Dynamics, and Control*, V07BT10A002-1–V07BT10A002-10. Portland, OR: ASME Design Engineering Div., ASME Computers and Information in Engineering Div.

Kłodowski, A., T. Rantalainen, A. Mikkola, A. Heinonen, and H. Sievänen. 2011. "Flexible multibody approach in forward dynamic simulation of locomotive strains in human skeleton with flexible lower body bones." *Multibody Syst. Dyn.* 25 (4): 395–409. https://doi.org/10.1007/s11044-010-9240-9.

Kreyszig, E. 1991. *Differential geometry.* New York: Dover.

Laflin, J. J., K. S. Anderson, I. M. Khan, and M. Poursina. 2014. "New and extended applications of the divide-and-conquer algorithm for multibody dynamics." *ASME J. Comput. Nonlinear Dyn.* 9 (4): 041004-1. https://doi.org/10.1115/1.4027869.

Lee, J.-H., and T.-W. Park. 2012. "Development and verification of a dynamic analysis model for the current-collection performance of high-speed trains using the absolute nodal coordinate formulation." *Trans. Korean Soc. Mech. Eng. A* 36 (3): 339–346. https://doi.org/10.3795/KSME-A.2012.36.3.339.

Li, S., Y. Wang, X. Ma, and S. Wang. 2019. "Modeling and simulation of a moving yarn segment: Based on the absolute nodal coordinate formulation." *Math. Probl. Eng.* 2019: 6567802. https://doi.org/10.1155/2019/6567802.

Logan, D. L. 2017. *A first course in the finite element method.* 6th ed. Boston: Cengage Learning.

LS-DYNA. 2018. *LS-DYNA keyword user's manual*. Livermore, CA: Livermore Software Technology Corporation.

Lubarda, V. A. 2004. "Constitutive theories based on the multiplicative decomposition of deformation gradient: Thermoelasticity, elastoplasticity, and biomechanics." *Appl. Mech. Rev.* 57 (2): 95–108. https://doi.org/10.1115/1.1591000.

Mikkola, A. M., and A. A. Shabana. 2003. "A non-incremental finite element procedure for the analysis of large deformation of plates and shells in mechanical system applications." *Multibody Syst. Dyn.* 9 (3): 283–309. https://doi.org/10.1023/A:1022950912782.

Nachbagauer, K. 2013. "Development of shear and cross section deformable beam finite elements applied to large deformation and dynamics problems." Ph.D. dissertation, Institute of Technical Mechanics, Johannes Kepler Univ.

Nachbagauer, K. 2014. "State of the art of ANCF elements regarding geometric description, interpolation strategies, definition of elastic forces, validation and locking phenomenon in comparison with proposed beam finite elements." *Arch. Comput. Methods Eng.* 21 (3): 293–319. https://doi.org/10.1007/s11831-014-9117-9.

Nachbagauer, K., A. S. Pechstein, H. Irschik, and J. Gerstmayr. 2011. "A new locking-free formulation for planar, shear deformable, linear and quadratic beam finite elements based on the absolute nodal coordinate formulation" *Multibody Syst. Dyn.* 26 (3): 245–263. https://doi.org/10.1007/s11044-011-9249-8.

Obrezkov, L., P. Eliasson, A. B. Harish, and M. K. Matikainen. 2021. "Usability of finite elements based on the absolute nodal coordinate formulation for deformation analysis of the Achilles tendon." *Int. J. Non Linear Mech.* 129 (103662): 1–11. https://doi.org/10.1016/j.ijnonlinmec.2020.103662.

Ogden, R. W. 1984. *Non-linear elastic deformations*. Mineola, NY: Dover.

Ojas, J., and P. Leyland. 2014. "Stability analysis of a partitioned fluid–structure thermal coupling algorithm." *J. Thermophys. Heat Transfer* 28 (1): 59–67. https://doi.org/10.2514/1.T4032.

Olshevskiy, A., O. Dmitrochenko, and C.-W. Kim. 2014. "Three-dimensional solid brick element using slopes in the absolute nodal coordinate formulation." *ASME J. Comput. Nonlinear Dyn.* 9 (2): 021001-1. https://doi.org/10.1115/1.4024910.

Orzechowski, G. 2012. "Analysis of beam elements of circular cross section using the absolute nodal coordinate formulation." *Arch. Mech. Eng.* 59 (3): 283–296. https://doi.org/10.2478/v10180-012-0014-1.

Orzechowski, G., and J. Fraczek. 2015. "nearly incompressible nonlinear material models in the large deformation analysis of beams using ANCF." *Nonlinear Dyn.* 82 (1): 451–464. https://doi.org/10.1007/s11071-015-2167-1.

Orzechowski, G., and J. Frączek. 2012. "Integration of the equations of motion of multibody systems using absolute nodal coordinate formulation" *Acta Mech. Autom.* 6 (2): 75–83.

Pan, K., and D. Cao. 2020. "Absolute nodal coordinate finite element approach to the two-dimensional liquid sloshing problems." *Proc. Inst. Mech. Eng. Part K: J. Multi-body Dyn.* 234 (2): 1–25. https://doi.org/10.1177/1464419320907785.

Perelman, T. L. 1961. "On conjugated problems of heat transfer." *Int. J. Heat Mass Transfer* 3 (4): 293–303. https://doi.org/10.1016/0017-9310(61)90044-8.

Piegl, L., and W. Tiller. 1997. *The NURBS book*. 2nd ed. Berlin: Springer.

Roe, B., A. Haselbacher, and P. H. Geubelle. 2007. "Stability of fluid–structure thermal simulations on moving grids." *Int. J. Numer. Methods Fluids* 54 (9): 1097–1117. https://doi.org/10.1002/fld.1416.

Roe, B., R. Jaiman, A. Haselbacher, and P. H. Geubelle. 2008. "Combined interface boundary method for coupled thermal simulations." *Int. J. Numer. Methods Fluids* 57 (3): 329–354. https://doi.org/10.1002/fld.1637.

Rogers, D. F. 2001. *An introduction to NURBS with historical perspective*. San Diego: Academic Press.

Rus, D., and M. T. Tolley. 2015. "Design, fabrication and control of soft robots." *Nature* 521: 467–475. https://doi.org/10.1038/nature14543.

Shabana, A. 1986. "Thermal analysis of viscoelastic multibody systems." *Mech. Mach. Theory* 21 (3): 231–242. https://doi.org/10.1016/0094-114X(86)90099-6.

Shabana, A. A. 2015. "Definition of ANCF finite elements." *ASME J. Comput. Nonlinear Dyn.* 10 (5): 054506-1. https://doi.org/10.1115/1.4030369.

Shabana, A. A. 2018. *Computational continuum mechanics*. 3rd ed. Cambridge, UK: Cambridge University Press.

Shabana, A. A., and H. Ling. 2019. "Noncommutativity of finite rotations and definitions of curvature and torsion." *ASME J. Comput. Nonlinear Dyn.* 14 (9): 091005-1. https://doi.org/10.1115/1.4043726.

Shen, Z., C. Liu, and H. Li. 2020. "Viscoelastic analysis of bistable composite shells via absolute nodal coordinate formulation." *Compos. Struct.* 248: 112537. https://doi.org/10.1016/j.compstruct.2020.112537.

Shen, Z., Q. Tian, X. Liu, and G. Hu. 2013. "Thermally induced vibrations of flexible beams using Absolute Nodal Coordinate Formulation." *Aerosp. Sci. Technol.* 29 (1): 386–393. https://doi.org/10.1016/j.ast.2013.04.009.

Spencer, A. J. M. 1980. *Continuum mechanics*. London: Longman.

Takahashi, Y., N. Shimizu, and K. Suzuki. 2005. "Study on the frame structure modeling of the beam element formulated by absolute Nodal coordinate approach." *J. Mech. Sci. Technol.* 19: 283–291. https://doi.org/10.1007/BF02916146.

Tian, Q., L. P. Chen, Y. Q. Zhang, and J. Z. Yang. 2009. "An efficient hybrid method for multibody dynamics simulation based on absolute nodal coordinate formulation." *ASME J. Comput. Nonlinear Dyn.* 4 (2): 021009-1. https://doi.org/10.1115/1.3079783.

Trivedi, D., D. Dienno, and C. D. Rahn. 2008. "Optimal, model-based design of soft robotic manipulators." *ASME J. Mech. Des.* 130 (9): 091402-1–091402-9. https://doi.org/10.1115/1.2943300.

Ukani, S. S., C. W. Chang and A. A. Shabana. 1988. "Thermoelastic analysis of flexible multi-body machine tool mechanisms." *ASME J. Mech. Transm. Autom. Des.* 110 (1): 48–55. https://doi.org/10.1115/1.3258904.

Vujosevic, L., and V. A. Lubarda. 2002. "Finite-strain thermoelasticity based on multiplicative decomposition of deformation gradient." *Theor. Appl. Mech.* 28–29: 379–399. https://doi.org/10.2298/TAM0229379V.

Yamano, A., A. Shintani, A. Ito, T. Nakagawa, and H. Ijima. 2020. "Influence of boundary conditions on a flutter-mill." *J. Sound Vib.* 478: 115359. https://doi.org/10.1016/j.jsv.2020.115359.

Yoo, W.-S., J.-H. Lee, S.-J. Park, J.-H. Sohn, D. Pogolev, and O. Dmitrochenko. 2004. "Large deflection analysis of a thin plate: Computer simulation and experiment." *Multibody Syst. Dyn.* 11 (2): 185–208. https://doi.org/10.1023/B:MUBO.0000025415.73019.bb.

Yu, L., Z. Zhao, J. Tang, and G. Ren. 2010. "Integration of absolute nodal elements into multibody system." *Nonlinear Dyn.* 62 (4): 931–943. https://doi.org/10.1007/s11071-010-9775-6.

Zienkiewicz, O. C. 1977. *The finite element method*. 3rd ed. New York: McGraw-Hill.

Zienkiewicz, O. C., and R. L. Taylor. 2000. *The finite element method, Vol. 2: Solid mechanics*. Oxford: Butterworth-Heinemann.